Study of (p, xn) Reactions at 400 MeV*

LARRY B. CHURCH† ‡ AND ALBERT A. CARETTO, JR.
Carnegie-Mellon University, Pittsburgh, Pennsylvania

(Received 23 May 1968)

Cross sections for a number of (p, xn) reactions ($1 \leq x \leq 4$) at 400 MeV are reported. The excitation function for the $Ge^{72}(p, xn)As^{73-x}$ system was measured between 100 and 400 MeV. The data are compared with the results of Monte Carlo cascade (Vegas) calculations and evaporation calculations. The experimental dependence of the $As^{75}(p, xn)Se^{76-x}$ cross sections on x did not agree well with the results of these calculations, although the Vegas step calculations reproduced the shape of this dependence. The cross-section data are consistent with a mechanism involving charge-exchange p-n scatterings, within the target nucleus, followed by the evaporation of $x-1$ neutrons. The ratio of $\sigma(p, 2n)$ to $\sigma(p, n)$ was found to be approximately linear with the quantity $E_{T_z}{}^*/S_n$. This quantity is the ratio of the excitation energy obtained if the isobaric analog state of the target is populated via the (p, n) reaction, to the neutron separation energy. On the basis of the postulated mechanism, the propability for charge-exchange scattering as a function of excitation energy was obtained for Y^{89} and Te^{126}.

INTRODUCTION

A NUMBER of detailed studies of (p, pn) and $(p, 2p)$ reactions have been reported[1] for incident protons above 100 MeV. Excitation functions for a number of (p, n) reactions at energies between 100 and 400 MeV have also been determined[2-4]; however, an equivalent study of (p, xn) reactions, where $x \geq 1$, has not been reported in this energy region.

These (p, xn) reactions are of interest primarily because the interaction probabilities leading to (p, xn) reaction products are severely limited mechanistically. The most likely mechanism for a (p, n) reaction involves those p-n, or charge-exchange, scatterings of the incident proton which lead to excitation energy less than about 10 MeV. The excitation energy, from interactions of this type, is the sum of the neutron "hole" energy and the energy of scattered proton above the proton Fermi energy. For those charge-exchange scatterings in which the excitation energy is greater than 10 MeV, the nucleus can de-excite by neutron or other particle evaporation.

For reactions where $x > 1$, the mechanism may involve larger laboratory angle p-n elastic scatterings such that for $(p, 2n)$ reactions the residual excitation energy lies between about 10 and 20 MeV, for $(p, 3n)$ reactions between about 20 and 30 MeV, etc. Therefore, this mechanism implies an elastic scattering of a neutron from the nuclear volume by a p-n interaction (a p-n cascade), followed by the evaporation of $x-1$ neutrons.

Alternatively, a mechanism may be visualized in which the incident proton engages in several collisions with neutrons, causing the eventual ejection of x neutrons and no other particles, and simultaneously depositing excitation energy less than about 10 MeV, or the ejection of less than x neutrons followed by nucleon evaporation. According to cascade Monte Carlo calculations, events of this type involving such a unique class of multiple scatterings are of very low probability, too low to account for the observed cross sections.[5,6]

It has been suggested[1] that the enhancement of the transition leading to the isobaric analog state may play an important role in comparisons of (p, n) and $(p, 2n)$ reactions. Valentin *et al.*[7] have measured (p, n) reaction cross sections at 155 MeV for a number of targets. In every case where the target and product ground states involve a $\Delta T = 0$ (isobaric-spin quantum-number change), the measured (p, n) cross sections were factors of 3 or 4 times larger than for those cases in which $\Delta T \neq 0$.

The objective of the work reported here was to obtain reliable cross sections for a number of target systems, to try to ascertain any particular trend that the data may display as a function of target mass or composition, and to test the consistency of these data with the various possible mechanisms.

EXPERIMENTAL

The cross sections were determined by conventional techniques, using the internal proton beam of the Carnegie-Mellon synchrocyclotron. The targets were usually bombarded at a radial position in a magnetic field which resulted in a proton energy of 400 ± 20 MeV. After the bombardment, the products were separated

* Work supported in part by the U.S. Atomic Energy Commission and the National Science Foundation.

† Presented in partial fulfillment of the Ph.D. degree in the Department of Chemistry, Carnegie Institute of Technology, Pittsburgh, Pa.

‡ Present address: State University of New York, Buffalo, New York.

[1] J. R. Grover and A. A. Caretto, Jr., Ann. Rev. Nucl. Sci. **14**, 51 (1964).

[2] W. J. Tretyl and A. A. Caretto, Jr., Phys. Rev. **146**, 836 (1966).

[3] R. C. Koch, Ph.D. thesis, University of Chicago, 1955 (unpublished).

[4] J. B. J. Read and J. M. Miller, Phys. Rev. **140**, B623 (1965).

[5] N. Metropolis, R. Bivins, M. Storm, A. Turkevich, J. M. Miller, and G. Friedlander, Phys. Rev. **110**, 185 (1958).

[6] K. Chen, Z. Fraenkel, G. Friedlander, J. R. Grover, J. M. Miller, and Y. Shimamoto, Phys. Rev. **166**, 949 (1968).

[7] L. Valentin, G. Albouy, J. P. Cohen, and M. Gusakow, Phys. Letters **7**, 163 (1963).

TABLE I. Target materials.

Nuclide	% abundance Natural	% abundance Enriched	% purity	Target composition	Average target thickness (mg/cm²)	Supplier[a]
Co^{59}	100	...	99.8	Co foil	110	A
Zn^{68}	...	99.3	99.95	ZnO+Al	90	B
Ge^{72}	...	96.4	99.8	$GeO_2+H_3BO_3$	45	B
As^{75}	100	...	99.99	As_2O_3+Al	120	C
Y^{89}	100	...	99.99	Y_2O_3	35	C
Zr^{90}	...	97.94	99.98	$ZrO_2+H_3BO_3$	50	B
Zr^{96}	...	80.03	99.9	$ZrO_2+H_3BO_3$	50	B
Te^{125}	...	95.0	99.9	Te+Al	68	B
Te^{126}	...	97.0	99.9	Te+Al	65	B
Hg^{202}	...	88.5	b	HgO+Al	62	B

[a] Suppliers: A, A. D. Mackay, Inc., New York; B, Oak Ridge National Laboratory, Oak Ridge, Tenn.; and C, Johnson, Mathey and Co., Ltd., London.
[b] Not given by supplier.

and purified, using standard radiochemical techniques.[8] A least-squares analysis of the decay curve was used to determine the activity of the product nuclides at the end of the proton bombardment.

The target materials, thicknesses, and their associated properties are summarized in Table I. With one exception, the targets were bombarded after being mixed with a binding material and compressed under a pressure of 40 tons per square inch to form a self-supporting pellet. The binding materials were either boric acid or aluminum powder; it was found that the boric acid generally gave superior pellets, but could not withstand as high a beam current compared to the aluminum pellet targets.

The average target thicknesses varied from 35 to 120 mg/cm², depending on the target system studied. The main drawback in the use of such relatively thick targets in a study of the (p, n) and $(p, 2n)$ reactions is the production of low-energy protons within the target. Since an inverse relationship exists between the proton energy and the (p, n) and $(p, 2n)$ cross sections,[2,9] the lower-energy protons produced within the target have a higher probability of causing a (p, n) or a $(p, 2n)$ reaction than the incident 400-MeV protons.

To determine the extent to which the target thickness affected this study, the cross sections of Nb^{90} and Nb^{89} were measured from naturally occurring zirconium in pellets of various thicknesses. Since naturally occurring zirconium consists of 51.5% Zr^{90}, it is felt that the Nb^{90} and Nb^{89} cross sections may represent the majority of the (p, n) and $(p, 2n)$ cross sections, respectively. It was found that the Nb^{89} cross sections appeared to be independent of pellet thickness, while the Nb^{90} had a positive slope of about 0.58 mb per 100 mg/cm² of pellet material. This represents a 13% increase per 100 mg/cm². This is in reasonable agreement with Koch,[3] who determined that the $Ni^{64}(p, n)Co^{64}$ cross section increased 18% per 100 mg/cm² of nickel foil. Thus, while it is believed that the (p, n) cross section is more dependent upon target thickness than the $(p, 2n)$ cross section, this effect is not serious enough to require a correction in reporting any of the measured cross sections.

A previously described[10] sedimentation targeting technique was used with the yttrium-oxide targets. It consisted of grinding the oxide to a fine consistency and filtering it onto a leveled glass filter paper from a slurry with ethyl alcohol. The filter paper and oxide were dried and weighed to determine the weight of the target material. The target was then covered by a thin layer of Duco cement. The oxide had a uniform appearance and good adherence to the glass filter paper.

During the bombardment all targets were flanked on each side by a set of aluminum foils consisting of an outer guard, a monitor foil, and an inner guard. The cross sections were determined relative to the cross sections of the $Al^{27}(p, 3pn)Na^{24}$ monitor reaction using the values suggested by Cumming.[11]

It was assumed that the $Al^{27}(p, 3pn)Na^{24}$ reaction was the only reaction producing Na^{24} in the 0.001-in. 99.99%-pure aluminum monitor foils. This assumption and the alignment between the target and monitor foils were checked by comparing the Na^{24} produced in each monitor foil. This difference in activity was usually less

[8] Subcommittee on Radiochemistry, *Monographs on the Radiochemistry of the Elements* (National Academy of Sciences–National Research Council, Washington, D.C. 20025), NAS-NS 3001-3058.
[9] N. T. Porile, Phys. Rev. **125**, 1379 (1962).
[10] N. T. Porile and L. B. Church, Phys. Rev. **133**, B310 (1964).
[11] J. B. Cumming, Ann. Rev. Nucl. Sci. **13**, 261 (1963).

TABLE II. Decay schematics.

Nuclide	Half-life	Radiation measured	Maximum energy (MeV)	Branching abundance
Ni^{57}	37 h	β^+	0.85	0.31[b]
		β^+	0.71	0.043
Ni^{56}	6.1 days[c]	Daughter		
Co^{56}	77.3 days	γ	1.24	0.63
Ga^{68}	68 min	β^+	1.89	0.86
		β^+	0.82	0.015
Ga^{67}	78 h	γ	0.296	0.22
Ga^{66}	9.5 h	β^+	4.153	0.512[d]
		β^+	0.935	0.03
As^{72}	26 h	β^+	3.34	0.174
		β^+	2.50	0.564
		β^+	1.84	0.03
As^{71}	62 h	β^+	0.812	0.35
As^{70}	52 min	β^+	2.14	0.75[e]
		β^+	1.89	0.06
		β^+	1.44	0.10
Se^{75}	120 days	γ	0.265 and 0.280	0.80[f]
Se^{73m}	36.5 min[g]	β^+	1.72	0.63[h]
		β^+	1.47	0.07
		β^+	0.89	0.02
Se^{73g}	7.1 h	β^+	1.32	0.699
Se^{73}	8.4 days	Daughter		
Zr^{89}	79 h	β^+	0.90	0.22[i]
		γ	0.92	1.00
Zr^{88}	85 days	γ	0.394	1.00
Zr^{87}	96 min[j]	β^+	2.10	0.83
Zr^{86}	16.5 h[k]	Daughter		
Y^{86}	15 h	β^+	1.96[l]	0.04
		β^+	1.19	0.15
		β^+	0.75	0.05
		β^+	0.63	0.03
Nb^{90}	14.6 h	γ	2.3	0.82
Nb^{89}	...	Daughter		
Nb^{88}	15 min[m]	Daughter		
Nb^{96}	23 h	β^-	0.37	0.08
		β^-	0.70	0.92
Nb^{95m}	90 h	x	0.016	0.91[j,n]
Nb^{95}	35 days	γ	0.76	1.00
I^{126}	13.1 days	β^-	1.25	0.093
		β^-	0.865	0.29
		β^-	0.385	0.058
I^{125}	60 days	x	0.035	1.80[n]
I^{124}	4.1 days	β^+	2.15	0.11
		β^+	1.51	0.14
I^{123}	13 h	x	0.035	1.15[n]
Tl^{202}	12 days	γ	0.440	0.954[o]
Tl^{201}	73 h	x	0.069	1.00

[a] Except where noted, all properties were taken from *Nuclear Data Sheets*, Compiled by K. Way *et al.* (Printing and Publishing Office, National Academy of Sciences–National Research Council, Washington, D. C. 20025), NRC 61-2-23 to 5-2-74.

[b] G. Chilosi, S. Monaro, and R. A. Ricci, Nuovo cimento **26**, 440 (1962).

[c] D. O. Wells, S. L. Blatt, and W. E. Meyerhof, Phys. Rev. **130**, 1961 (1963).

[d] D. C. Camp and L. M. Langer, Phys. Rev. **129**, 1782 (1963).

[e] P. Born, C. Bobeldijk, W. A. Oost, and J. Blok, Physica **29**, 277 (1963).

[f] E. P. Grigoriev and A. V. Zolotavin, Nucl. Phys. **14**, 443 (1963).

[g] J. B. Cumming (private communication).

[h] R. A. Ricci, R. van Lieshout, and H. S. van den Bold, Physica **26**, 1014 (1960).

[i] D. M. Van Patter and S. M. Shafroth, Nucl. Phys. **50**, 113 (1964).

[j] Determined as part of this study.

[k] E. K. Hyde, W. J. Treytl, A. Siivola, D. H. Sisson, and D. K. Horen, Phys. Rev. **142**, 657 (1966).

[l] T. Yamazaki, H. Ikegami, and M. Sakai, Nucl. Phys. **30**, 68 (1962).

[m] R. G. Korteling and E. K. Hyde, Phys. Rev. **136**, B425 (1964).

[n] The branching abundances of the x rays do not include the fluorescence yield.

[o] W. H. G. Lewin, J. Bezemer, and C. W. E. Van Eijk, Nucl. Phys. **62**, 337 (1965).

than 2.5% of the average activity of the two monitor foils. All of the guard foils were 99.99%-pure 0.0004-in.-thick aluminum foil. The outer guards protected the target stack from stray recoils during bombardment and compensated for the Na^{24} atoms recoiling out of the adjacent monitor foils. After bombardment they were discarded. The two inner aluminum guards caught recoils originating in the target and compensated for the Na^{24} recoiling out of the monitor foils. The inner guards were dissolved with the target.

In order to determine the activity of each product nuclide which may have come from the aluminum guard foils and binding materials, a blank target was irradiated for each product. In all cases the activity of the product nuclide in the blank runs was negligible and was therefore ignored.

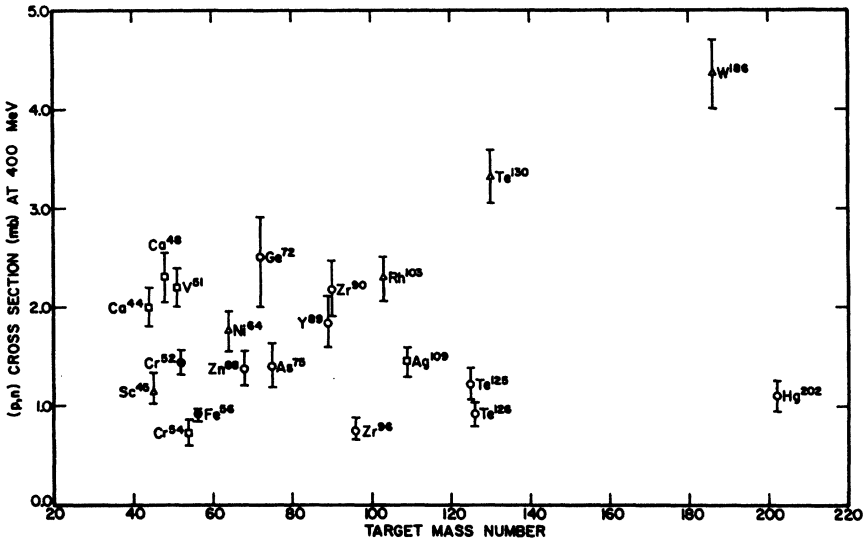

FIG. 1. Cross sections of (p, n) reactions at 400 MeV versus target mass number. ○, this work; ●, Ref. 18; □, Ref. 4; △, Ref. 2.

After the irradiation, the target was dissolved in the presence of the appropriate carriers and the necessary chemistry performed to ensure a pure sample.[12] The final precipitate of the product was filtered onto filter paper and dried. The precipitate and filter paper were then mounted on an aluminum card and covered with 1-mg/cm^2 polyethylene foil.

The decay rates of most of the products which decayed with the emission of β radiation were determined by counting with an end-window, methane-flow proportional counter which was calibrated for absolute counting, using a procedure reported by Bayhurst and Prestwood.[13] The calibration is felt to be accurate to within 8% of the given efficiency.

In products where the γ radiations were detected, a 3×3-in. NaI(Tl) crystal was used in connection with a photomultiplier tube and a multichannel analyzer. The γ count rate was converted to the disintegration rate by a procedure reported by Heath.[14]

A very thin (2 mm) NaI(Tl) crystal was used to detect x rays. Its efficiency was determined by counting commercially available standards whose x-ray energy was the same or very close to the x-ray energy of the product being counted.

A summary of the radiation measured for each product nuclide and other important decay scheme data is presented in Table II.

RESULTS

Cross sections were calculated from the measured values of the activities by the standard procedure. These cross sections and the associated uncertainties are listed in Table III.

The total random uncertainty R of the individual determinations was estimated using either the standard deviation of the individual determinations, or the square root of the sum of the squares of the estimated random uncertainties, whichever was larger. Included in the random uncertainties were the uncertainties of target and monitor masses, the decay curve resolutions, and the chemical yields. The total systematic uncertainties S, listed in Table III, are the square root of the sum of the squares of the systematic uncertainties encountered in measuring the cross sections. These include uncertainties such as those associated with the monitor cross section and the decay scheme of a product nuclide. The total uncertainty T was calculated by combining the systematic uncertainty and the random uncertainty by $T=(S^2+R^2/N)^{1/2}$.

The $Te^{125}(p, xn)I^{126-x}$ cross sections were corrected for the contribution due to the 3.21 at.% of Te^{126} contained in the enriched Te^{125} target. The $Te^{126}(p, xn)I^{127-x}$ cross sections listed in Table III were used to make these corrections, which averaged about 5%. Similar corrections should be applied to the $Hg^{202}(p, xn)Tl^{203-x}$ cross sections, due to the 1.55% Hg^{204}, 3.56% Hg^{201}, and 3.73% Hg^{200} in the enriched Hg^{202} target. However, this is not possible at the present time, because of the lack of (p, xn) cross sections on these mercury isotopes.

Several cross sections in Table III have been previously measured at or near 400 MeV. It is somewhat distressing that there is often poor agreement between the different determinations of the same cross section at the same bombarding energies by experimenters in different laboratories. For example, Levenberg *et al.*[15] have recently measured the (p, n) and $(p, 2n)$ cross section of Y^{89} at 400 MeV. They have determined both cross sections to be about 25% higher than the values

[12] L. B. Church, Ph.D. thesis, Carnegie Institute of Technology, 1966 (unpublished).
[13] B. P. Bayhurst and R. J. Prestwood, Nucleonics **17**, 82 (1959).
[14] R. L. Heath, U.S. Atomic Energy Commission Research and Development Report No. IDO-16880-1, 1964 (unpublished).
[15] I. Levenberg, V. Pokrovsky, L. Tarasova, Van Cheng-Peng, and I. Yutlandov, Nucl. Phys. **81**, 81 (1966).

TABLE III. Experimentally measured cross sections.

Reaction	Energy (Mev)	Cross section and total uncertainty (mb)	Number of individual determinations	Total random uncertainty (%)	Total systematic uncertainty (%)
$Co^{59}(p, 3n)Ni^{57}$	400	0.462±0.116	2	4.5	25
$Co^{59}(p, 4n)Ni^{56}$	400	0.0065±0.0010	2	3.9	16
$Zn^{68}(p, n)Ga^{68}$	400	1.38±0.18	2	5.5	13
$Zn^{68}(p, 2n)Ga^{67}$	400	2.34±0.34	2	9.6	13
$Zn^{68}(p, 3n)Ga^{66}$	400	2.30±0.35	2	10.0	14
$Ge^{72}(p, n)As^{72}$	400	2.46±0.45	2	9.0	17
$Ge^{72}(p, 2n)As^{71}$	400	3.81±0.62	2	9.0	15
$Ge^{72}(p, 3n)As^{70}$	400	1.96±0.36	2	3.5	18
$Ge^{72}(p, n)As^{72}$	300	3.12±0.54	2	3.5	17
$Ge^{72}(p, 2n)As^{71}$	300	5.59±0.85	2	3.5	15
$Ge^{72}(p, 3n)As^{70}$	300	2.82±0.51	2	3.5	18
$Ge^{72}(p, n)As^{72}$	200	5.03±0.89	2	7.3	17
$Ge^{72}(p, 2n)As^{71}$	200	8.58±1.36	2	5.1	15
$Ge^{72}(p, 3n)As^{70}$	200	5.01±0.91	2	3.5	18
$Ge^{72}(p, n)As^{72}$	100	10.29±2.02	2	13.8	17
$Ge^{72}(p, 2n)As^{71}$	100	18.77±3.21	2	11.6	15
$Ge^{72}(p, 3n)As^{70}$	100	10.23±1.86	2	3.5	18
$As^{75}(p, n)Se^{75}$	400	1.40±0.23	3	6.4	16
$As^{75}(p, 3n)Se^{73m}$	400	0.52±0.11	3	13.2	21
$As^{75}(p, 3n)Se^{73g}$	400	3.80±0.57	3	13.1	13
$As^{75}(p, 3n)Se^{73}$ (total)	400	4.32±1.12	3	18.4	25
$As^{75}(p, 4n)Se^{72}$	400	1.82±0.38	2	18.6	16
$Y^{89}(p, n)Zr^{89}$	400	1.85±0.27	3	6.9	14
$Y^{89}(p, 2n)Zr^{88}$	400	4.51±0.52	3	6.2	11
$Y^{89}(p, 3n)Zr^{87}$	400	3.85±0.70	3	5.8	18
$Y^{89}(p, 4n)Zr^{86}$	400	2.39±0.38	3	12.4	14
$Zr^{90}(p, n)Nb^{90}$	400	2.18±0.29	3	10.4	12
$Zr^{90}(p, 2n)Nb^{89}$	400	3.52±0.64	3	12.0	17
$Zr^{90}(p, 3n)Nb^{88}$	400	3.79±0.95	3	3.0	25
$Zr^{96}(p, n)Nb^{96}$	400	0.76±0.12	2	13.0	13
$Zr^{96}(p, 2n)Nb^{95m}$	400	3.85±0.64	2	10.5	15
$Zr^{96}(p, 2n)Nb^{95}$ (total)	400	4.45±0.61	2	11.4	11

TABLE III (*Continued*)

Reaction	Energy (MeV)	Cross section and total uncertainty (mb)	Number of individual determinations	Total random uncertainty (%)	Total systematic uncertainty (%)
$Te^{125}(p, n)I^{125}$	400	1.23±0.16	2	8.7	12
$Te^{125}(p, 2n)I^{124}$	400	3.12±0.40	3	8.0	12
$Te^{125}(p, 3n)I^{123}$	400	2.09±0.25	3	10.0	11
$Te^{126}(p, n)I^{126}$	400	0.92±0.12	4	8.0	13
$Te^{126}(p, 2n)I^{125}$	400	3.33±0.41	4	6.4	12
$Te^{126}(p, 3n)I^{124}$	400	3.52±0.44	4	6.4	12
$Te^{126}(p, 4n)I^{123}$	400	2.50±0.32	4	6.7	11
$Hg^{202}(p, n)Tl^{202}$	400	1.10±0.16	2	10.0	14
$Hg^{202}(p, 2n)Tl^{201}$	400	3.80±0.58	2	11.5	13

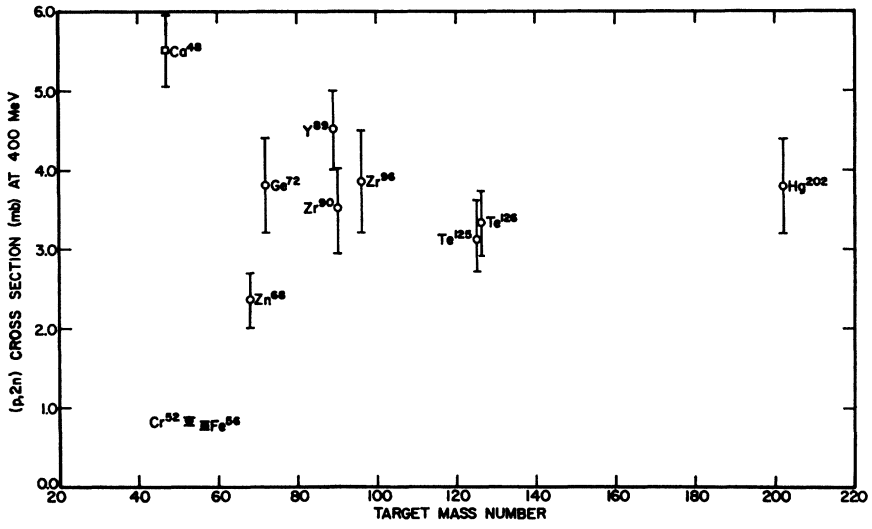

FIG. 2. Cross sections of $(p, 2n)$ reactions at 400 MeV versus target mass number. ○, this work; □, Ref. 4; ●, Ref. 18.

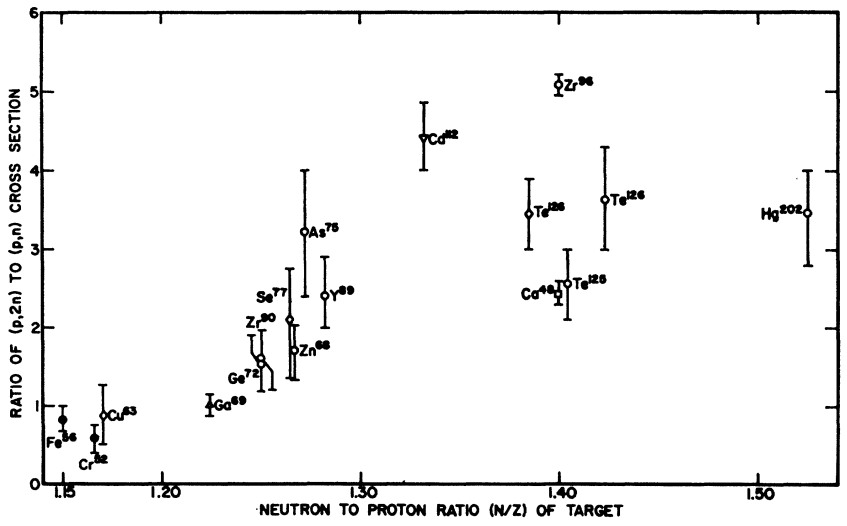

FIG. 3. Ratio of the $\sigma(p, 2n)/\sigma(p, n)$ versus the neutron to proton ratio of target. ○, this work; ●, Ref. 18; ◇, Ref. 19; △, W. J. Nieckarz (private communication); □, Ref. 4.

TABLE IV. Results of Vegas calculations for $(\tilde{p}, \tilde{n})$ and $(\tilde{p}, 2\tilde{n})$ cascades.

Target	E_i (MeV)	Number of cascades	STEP $(\tilde{p}, \tilde{n})$ $E^*<10$	STEP $(\tilde{p}, \tilde{n})$ $10<E^*<20$	STEP $(\tilde{p}, 2\tilde{n})$ $E^*<10$	STEP-NO $(\tilde{p}, \tilde{n})$ $E^*<10$	STEP-NO $(\tilde{p}, \tilde{n})$ $10<E^*<20$	STEP-NO $(\tilde{p}, 2\tilde{n})$ $E^*<10$
Ca^{40}	400	7 757	14	33	5	...	...	...
Co^{59}	160	10 000	...	...	...	84	106	4
Cu^{64}	400	2 000	6	11	...	9	8	...
As^{75}	375	3 000	9	12	2	14	12	1
Bi^{309}	375	3 000	10	12	1	11	16	1
U^{238}	155	9 900				61	95	3

listed in Table III. Although identical decay schemes, half-lives, and monitor cross sections were used in each case, a possible explanation for the discrepancy is that Levenberg *et al.* used targets of about 500 mg/cm^2 thickness. Thus it is not surprising that both the (p, n) and $(p, 2n)$ cross sections as determined by Levenberg *et al.* are significantly higher. However, in view of relative effects of target thickness on the (p, n) cross section as compared to the $(p, 2n)$ cross section, it is surprising that the $(p, 2n)$ to (p, n) cross-section ratios for the two determinations are approximately equal.

The $Zr^{96}(p, 2n)Nb^{95}$ cross section found in Table III is about $\frac{1}{3}$ as large as the same cross section reported by Strohal and Caretto.[16] The source of this difference is believed to be the method of counting. As was previously listed in Table II, the decay rate of the Nb^{95} was determined in this work by counting the 0.765-MeV γ ray. Strohal and Caretto counted the Nb^{95} with a Geiger-Müller tube. Because Nb^{95} has such a low β decay energy, $E_{max}=0.16$ MeV, an accurate determination of the counting efficiency of a Geiger-Müller tube would be extremely difficult using the semiempirical method reported by Strohal and Caretto.

Zaitseva *et al.*[17] have determined the (p, n), $(p, 2n)$, and $(p, 3n)$ cross sections on Te^{126} and the $(p, 2n)$ and $(p, 3n)$ cross sections on Te^{125} at 300, 480, and 660 MeV. When interpolated to 400 MeV, these cross sections are in fairly close agreement with those of Table III for all but the $Te^{126}(p, 2n)I^{125}$ cross section. (The results leading to an I^{124} product were normalized to the same β-decay branching abundance of I^{124} which is listed in Table II.) When interpolated to 400 MeV, these workers determined the $Te^{126}(p, 2n)I^{125}$ cross section to be 1.5±0.6 mb; this is to be compared to the 3.33±0.34-mb cross section listed in Table III. The reason for this large discrepancy is not clear, but it is difficult to compare the two determinations, since Zaitseva *et al.* did not clearly list the branching abundance used in their determination of the decay rate of I^{125}.

DISCUSSION

Two general conclusions can be drawn from the (p, n) and $(p, 2n)$ cross sections given in Table III: (i) both (p, n) and $(p, 2n)$ cross sections exhibit large and abrupt variations within a narrow range of target mass numbers, and (ii) the magnitude of the $\sigma(p, 2n)/\sigma(p, n)$ ratio is greater than unity for all the reported values.

The (p, n) and $(p, 2n)$ cross sections are plotted versus target mass number in Figs. 1 and 2 and the $\sigma(p, 2n)/\sigma(p, n)$ ratio versus the target N/Z in Fig. 3. Included in these figures are the results of other measurements at the same proton energy. These other points seem to enhance the scatter. However, the $\sigma(p, 2n)/\sigma(p, n)$ ratios for three of these—Cr^{52}, Fe^{56}, and Cu^{63}—are less than unity.[18,19]

The most plausible mechanism for (p, xn) reactions $(x\geq 1)$ at incident energies greater than 100 MeV involves a p-n scattering within the nucleus, or a charge-exchange scattering, such that the scattered proton receives a terminal kinetic energy (above the proton Fermi energy) between 0 and about 10 MeV for (p, n) reactions, between 10 and about 20 MeV for $(p, 2n)$ reactions, etc. Thus, for a $(p, 2n)$ reaction, the residual excitation energy from the p-n scattering must be within the energetic restrictions permissible for the evaporation of one neutron, within the energetic restrictions permissible for the evaporation of two neutrons for $(p, 3n)$ reactions, etc.

An alternative mechanism for $(p, 2n)$ reactions involving multiple scattering of the incident proton such that two neutrons are promptly ejected and the residual excitation is less than about 10 MeV seems particularly improbable. Such an interaction can be referred to as a $(\tilde{p}, 2\tilde{n})$ cascade.[20] The results of the recent Vegas Monte

[16] P. P. Strohal and A. A. Caretto, Jr., Phys. Rev. **121**, 1815 (1961).

[17] N. G. Zaitseva, M. Ya. Kuznetsova, M. N. Buk, and V. A. Khalkin, Zh. Eksperm. i Teor. Fiz. **43**, 1672 (1962) [English transl.: Soviet Phys.—JETP **16**, 1180 (1963)].

[18] L. P. Remsberg and J. M. Miller, Phys. Rev. **130**, 2069 (1963).

[19] D. J. Reuland (private communication).

[20] Intranuclear cascades, designated by $(\tilde{p}, \tilde{n})$, $(\tilde{p}, 2\tilde{n})$, etc. do not refer to the over-all reaction, which is represented by the conventional lower case letters.

Carlo calculations[6] provide an estimate of the extent of $(p, 2n)$ cascades leaving the nucleus with less than about 10 MeV of excitation. The Vegas calculation takes into account the radial variations of the nuclear density by dividing the nucleus into seven concentric zones or steps of constant density. Refraction and reflections of the incident and cascade particles at the interfaces of these zones are included in the calculation. This is referred to as the STEP cascade calculation. The STEP-NO calculation does not take into account refraction and reflection of the incident and cascade particles. The number of (p, n) and $(p, 2n)$ cascades observed for low residual excitation energies is indicated in Table IV. The results listed are for 2000 to 10 000 incident protons of 155 to 400 MeV incident on a series of targets. Within statistics, the number of $(p, 2n)$ cascades in which the residual excitation energy is less than 10 MeV is never larger than 0.07% of the number of incident protons. For the STEP version of the cascade calculation, this number is at least six times smaller than the number of (p, n) cascades in which the residual excitation energy is between 10 and 20 MeV and, for the STEP-NO calculation the number of appropriate $(p, 2n)$ cascades is never more than about 8% of the appropriate (p, n) cascades. Thus, such multiple scattering processes are not the dominant mechanism for $(p, 2n)$ reactions.

The excitation functions for the $Ge^{72}(p, xn)As^{73-x}$ reactions are illustrated in Fig. 4. In this figure $\ln\sigma(p, xn)$ is plotted versus $\ln E_i$. Also illustrated in this figure is the dependence of the elementary free p-n scattering cross section on incident energy plotted in the same fashion.[21] Note from the slopes of the elementary p-n cross section that its energy dependence varies from about E^{-1} to $E^{-0.5}$ between 100 and 400 MeV, while the slopes of these three (p, xn) excitation functions are essentially constant with energy and give an energy dependence between $E^{-1.03}$ and $E^{-1.19}$ for the three reactions. As pointed out by Grover and Caretto[1] and experimentally illustrated by Treytl and Caretto[2], the energy dependence of (p, n) reactions becomes weaker with increasing target mass number, presumably because of the increase in attenuation of the incident and outgoing nucleon waves with the large mass targets. An interpolation of the slope of the (p, n) excitation function for Ge^{72} from the data of Treytl and Caretto yields a predicted energy dependence for this reaction of $E^{-1.08}$ which compares well with the experimental value reported here of $E^{-1.03}$.

The similarity of the slopes of these three excitation functions is further evidence that the mechanism of (p, xn) reactions involves a p-n scattering followed by the evaporation of $x-1$ neutrons. Furthermore, it is apparent that the p-n cascade determines the energy dependence, while the probability of evaporating $x-1$ neutrons is approximately independent of incident

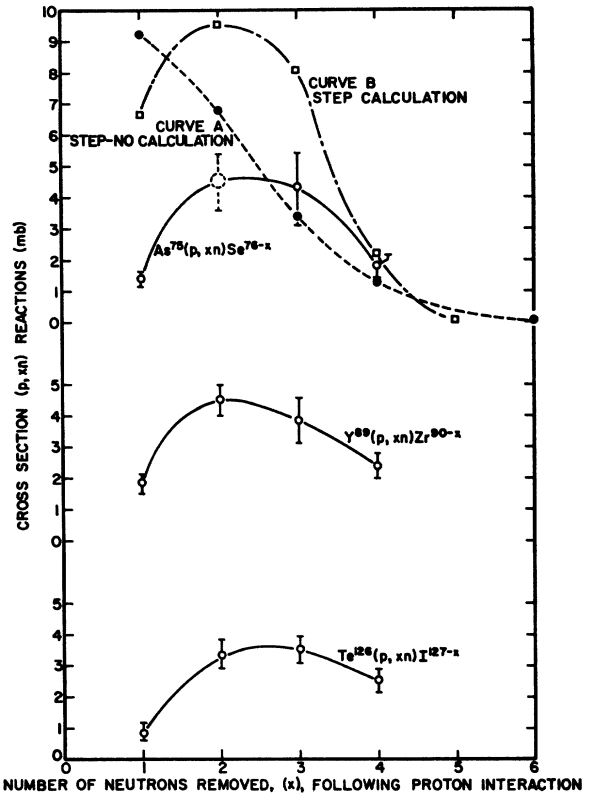

FIG. 5. Cross section of (p, xn) reactions at 400 MeV versus x, the number of neutrons removed following the initial p-n interaction. Calculations for the As^{75} target are for 378-MeV incident protons: Curve A results from the STEP-NO Vegas Monte Carlo cascade calculation with evaporation, and curve B results from the STEP Vegas Monte Carlo cascade calculation with evaporation.

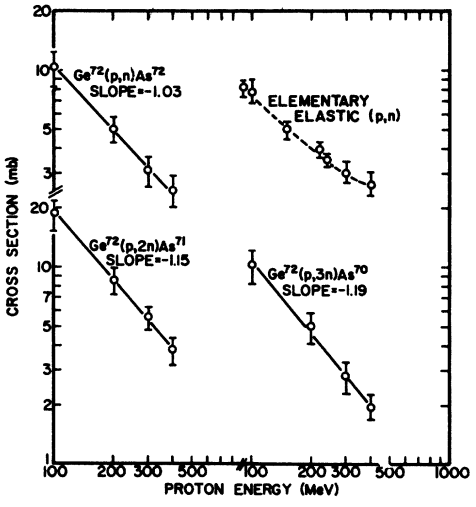

FIG. 4. Excitation functions of the $Ge^{72}(p, xn)As^{73-x}$ reactions. Also illustrated is the elementary p-n elastic cross section between 90 and 400 MeV. The slope of this curve on a $\ln\sigma$ versus $\ln E_i$ plot is not constant but varies from about -1.0 to about -0.5. Data for the elementary p-n elastic scattering cross section was taken from Ref. 21.

[21] W. N. Hess, Rev. Mod. Phys. **30**, 368 (1958).

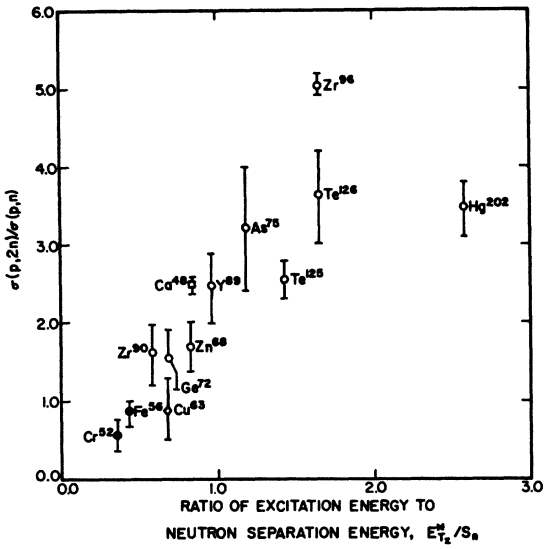

FIG. 6. The $\sigma(p, 2n)/\sigma(p, n)$ ratio versus $E_{T_z}{}^*/S_n$. See text for meaning of symbols. ○, this work; ◇, Ref. 19; □, Ref. 4.

energy. Particle evaporation is strongly dependent on the residual excitation energy spectrum, which is in turn dependent on the incident energy. However, for (p, xn) reactions, the fraction of the total excitation energy spectrum involved in the evaporation of the $x-1$ neutrons remains roughly constant with changing incident energy.

In Fig. 5 the variation of $\sigma(p, xn)$ at 400 MeV versus x is illustrated for As^{75}, Y^{89}, and Te^{126} targets. The value of the $As^{75}(p, 2n)Se^{74}$ cross section was interpolated on the basis of assuming that the $As^{75}(p, xn)Se^{76-x}$ reactions had a dependence on x similar to those for the other targets. Also indicated in this figure are the results of Vegas Monte Carlo cascade calculations on As^{75}, for 378-MeV incident protons, together with a Monte Carlo calculation of the evaporation probability from the residual excited nuclei resulting from the cascade process. Nucleon evaporation probabilities were calculated by means of an evaporation program[22] similar to that of Dostrovsky *et al.*,[23] using the Carnegie-Mellon University CDC-G21 computer. The Vegas results were obtained by calculating the number of cascades of different types at different residual excitation energies using 3000 incident protons of 378-MeV incident energy on As^{75}. For both the STEP and STEP-NO calculations, the only (p, xn) product observed at any excitation energy was Se^{75}. For the STEP calculations, there were 145 $(\tilde{p}, \tilde{n})$ cascades out of 3000 incident particles. For the STEP-NO calculations, there was a total of 67 $(\tilde{p}, \tilde{n})$ cascades out of 3000. For each case, 10 evaporation calculations were performed and the results of all the $(\tilde{p}, \tilde{n})$ cascades combined. Curve A in Fig. 5 is the result of the STEP-NO calculation plus evaporation and curve B the results of the STEP cascade calculation with evaporation. It is evident that the STEP cascade calculation reproduces the trend much more closely than do the STEP-NO results. On the other hand, the magnitudes of the cross sections are consistently high from the STEP calculation and, furthermore, the differences between the magnitudes of the calculated cross sections and the experimental values are greater for the STEP calculations than for the STEP-NO for all cases except $As^{75}(p, n)Se^{75}$. It is well known that Monte Carlo cascade calculations do not accurately reproduce the cross sections for simple reactions such as the (p, pn) and $(p, 2p)$ reactions. Simple reactions of this type, of which the (p, n) is a member, are probably very sensitive to parameters involving the target's nucleon configuration, and hence this lack of agreement is not surprising.

Based on the preceding evidence, it is reasonable to conclude that the dominant mechanism for (p, xn) reactions involves an intranuclear p-n scattering in which from zero to $x-1$ neutrons are evaporated depending on the residual excitation energy. Using the notation of Remsberg and Miller,[18] the ratio $\sigma(p, 2n)/\sigma(p, n)$ can be expressed by

$$\frac{\sigma(p, 2n)}{\sigma(p, n)} = \int_{\pi/2}^{\pi} \left(\frac{d\sigma}{d\Omega}\right)_{p,n} W(\theta)_1 P_{1n}(\theta) \sin\theta d\theta \Big/ \int_{\pi/2}^{\pi} \left(\frac{d\sigma}{d\Omega}\right)_{p,n} W(\theta)_0 P_{0n}(\theta) \sin\theta d\theta, \quad (1)$$

where $(d\sigma/d\Omega)_{p,n}$ is the p-n differential scattering cross section and θ is the c.m. scattering angle. For p-n scattering in which the proton retains less than the kinetic energy needed to escape, the scattering angle θ is between $\frac{1}{2}\pi$ and π. The lowest value of the kinetic energy of the scattered proton requires the largest scattering angles permissible. $W(\theta)_{x-1}$ is the probability that a collision with a scattering angle θ results in an energy transfer appropriate to the evaporation of $x-1$ neutrons. The probabilities of zero- or one-neutron evaporation are given by the terms $P_{0n}(\theta)$ and $P_{1n}(\theta)$, respectively, and are dependent on the residual excitation energy via the c.m. scattering angle θ.

Calculations of the terms $W(\theta)$ are currently underway,[24] using relativistic kinematics. The probability of a given type of energy transfer is calculated by varying systematically (i) the bound neutron kinetic energy before collision E_n between zero and the maximum Fermi energy E_f, (ii) the angle of the initial neutron momentum w with the proton beam, (iii) the c.m. plane angle ϕ, and (iv) the c.m. scattering angle θ.

[22] F. M. Kiely, Ph.D. thesis, Carnegie Institute of Technology, 1967 (unpublished).
[23] I. Dostrovsky, Z. Fraenkel, and G. Friedlander, Phys. Rev. **116**, 683 (1959).
[24] A. C. Stalker (private communication).

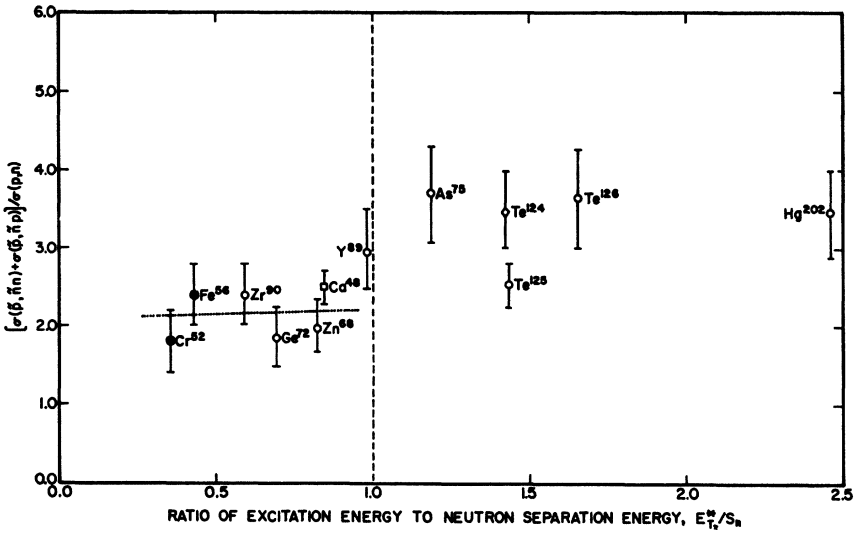

FIG. 7. The

$[\sigma(\tilde{p}, \tilde{n}n)+\sigma(\tilde{p}, \tilde{n}p)]/\sigma(p, n)$

ratio versus $E_{T_z}{}^*/S_n$. See text for meaning of symbols. ○, this work; ●, Ref. 18; □, Ref. 4; ◇, Ref. 19. Dotted line is least-squares fit of data to the left of dashed line at $E_{T_z}{}^* = S_n$.

Qualitative results indicate that, for $E_n = E_f$, $W(\theta)_0$ is slightly less than $W(\theta)_1$ at all angles θ except for $\theta > 160°$, in which region $W(\theta)_0$ is two to four times the value of $W(\theta)_1$. However, for values of E_n less than E_f, $W(\theta)_0$ decreases rapidly in absolute value and the range of angles for which values of $W(\theta)_0$ exist decreases rapidly toward π. Thus, at minimum energy transfers, for a (p, n) reaction, the integral of $W(\theta)_0$ between $\frac{1}{2}\pi$ and π exceeds that of $W(\theta)_1$. With increasing energy transfer, i.e., a $(p, 2n)$ reaction, the integral of $W(\theta)_1$ between $\frac{1}{2}\pi$ and π exceeds that of $W(\theta)_0$.

For convenience, let the function of $W(\theta)$ $(d\sigma/d\Omega)$ $\sin\theta$ be defined by $f(\theta)$. Values of $f(\theta)$ for large excitation energies are larger than for small excitation energies. Thus, one would expect that the $\sigma(p, 2n)/\sigma(p, n)$ ratio should be greater than unity for all targets at a given incident energy. The fact that this ratio for Cr^{52}, Fe^{56}, and Cu^{63} is less than unity can be attributed to the fact that proton evaporation competes successfully with neutron evaporation for the (p, n) products Mn^{52}, Co^{56}, and Zn^{63}, respectively, due to the low proton binding energies in these nuclei. Thus, since P_{0N} and P_{1N} vary from target to target, but in general have a smaller variation than the dependence of $f(\theta)$ on excitation energy, the ratio of $\sigma(p, 2n)/\sigma(p, n)$ might be expected to vary around some constant value. In Fig. 6 this ratio is plotted versus the quantity $E_{T_z}{}^*/S_n$. The excitation energy $E_{T_z}{}^*$ is the energy available for excitation if the isobaric analog state of the target is populated. This number is obtained from $E_{T_z}{}^* = E_c - |Q_{p,n}|$, where the Coulomb displacement energy[25] E_c is given by $E_c = \frac{3}{5}(e^2/R)[(2Z+1) - \frac{4}{3}(1.06)(Z+\frac{1}{2})^{1/3}]$ and $Q_{p,n}$ is the Q value for the (p, n) reaction to the ground state of the product. S_n is the neutron separation energy and R is given by $1.25\ A^{1/3}$ F.

As apparent from Fig. 6, the $\sigma(p, 2n)/\sigma(p, n)$ ratio increases approximately linearly with $E_{T_z}{}^*/S_n$. This result is consistent with transitions in which the population of the isobaric analog state of the target is enhanced. As the atomic number of the target increases, the Coulomb displacement energy E_c increases. To reach this state in the (p, n) product as the atomic number of the target increases involves p-n interactions at smaller c.m. scattering angles (in the second quadrant). At the smaller c.m. scattering angles, the term $W(\theta)$ is larger, thus causing an increase in events leading to neutron evaporation and hence an increase in $\sigma(p, 2n)$. The fact that the $\sigma(p, 2n)/\sigma(p, n)$ ratio is approximately linear with respect to $E_{T_z}{}^*/S_n$, for all known measurements, seems to imply that the population of the isobaric analog state is involved.

The ratio of the probability for the evaporation of one and only one proton to the probability for the evaporation of one and only one neutron, $G(p)/G(n)$, was calculated as a function of excitation energy for nuclei resulting from $(\tilde{p}, \tilde{n})$ interactions on most of the targets presented in Fig. 6. These calculations were performed using the evaporation program mentioned previously and for excitation energy intervals of 1 MeV from about 5 to 15 MeV and then 5-MeV intervals up to 50 or 60 MeV.

The experimentally measured $\sigma(p, 2n)/\sigma(p, n)$ ratios were corrected by the calculated $G(p)/G(n)$ ratios to yield an estimate of the ratio of total one-nucleon evaporation following $(\tilde{p}, \tilde{n})$ events to cases involving γ de-excitation following $(\tilde{p}, \tilde{n})$ events; namely, the quantity $[\sigma(\tilde{p}, \tilde{n}n)+\sigma(\tilde{p}, \tilde{n}p)]/\sigma(p, n)$ was calculated, and is plotted versus $E_{T_z}{}^*/S_n$ in Fig. 7. Values of this ratio for $E_{T_z}{}^*/S_n$ less than 1.0, vary between about 2.0 and 2.2 (dotted line). All the values of $[\sigma(\tilde{p}, \tilde{n}n)+\sigma(\tilde{p}, \tilde{n}p)]/\sigma(p, n)$ for $E_{T_z}{}^*/S_n$ greater than 1.0 are about a factor of 1.5 to 1.8 times larger than the values of this ratio at $E_{T_z}{}^*/S_n$ less than unity. The only point

[25] C. J. Batty, R. S. Gilmore, and G. H. Stafford, Nucl. Phys. 75, 599 (1966).

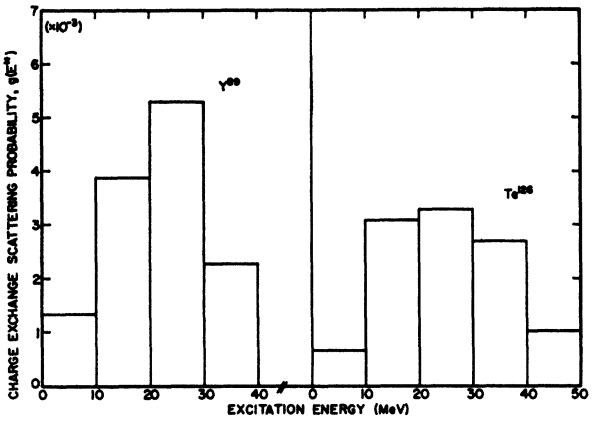

FIG. 8. Probability of charge-exchange scattering versus residual excitation energy for 400-MeV incident protons on Y^{89} and Te^{126}.

which appears as an anomaly is that for the Te^{125} data. The discontinuity at $E_T{}^*/S_n$ equal to unity is consistent with what would be predicted if the production of the isobaric analog state is enhanced in these reactions.

The differential cross section $(d\sigma/d\Omega)_{p,n}$ employed in Eq. (1) can be transformed to an equivalent dependence on excitation energy by an appropriate transformation,[4] $t(\theta, W)$. If a new function $g(E^*)$ is defined by $g(E^*) = t(\theta, W)f(\theta)$, where $f(\theta)$ is the same as previously defined, then $\sigma(p, xn)$ can be written

$$\sigma(p, xn) = \int_0^{E_i} g(E^*) P_{E(x-1)n} dE^*, \qquad (2)$$

where the function $g(E^*)$ is proportional to the probability of a p-n charge-exchange scattering as a function of excitation energy. $P_{E(x-1)n}$ is the neutron evaporation probability as defined previously. The experimental (p, xn) cross sections for Y^{89} and Te^{126} were used in Eq. (2) to evaluate the function $g(E^*)$. Values of the cross section for $(p, 5n)$ reactions were estimated by extrapolation of the curves in Fig. 5 to $x=5$. Neutron evaporation probabilities were calculated by the evaporation program previously mentioned. These quantities were evaluated for excitation energy intervals of 1 MeV from about 5 to 15 MeV and then 5-MeV intervals up to 50 MeV. A histogram of the probability of charge-exchange scattering $g(E^*)$ plotted versus excitation energy is illustrated in Fig. 8. Within experimental uncertainties, both histograms are fairly similar and indicate that the highest probability for successful p-n collisions occurs for cases when the residual excitation energy is between 20 and 25 MeV. The distribution for Te^{126} is broader than that for Y^{89}. This is probably related to the somewhat lower neutron binding energies in the iodine product nuclides as compared to the zirconium product nuclides. Thus, for a given value of x for (p, xn) reactions resulting from a charge-exchange scattering, nearly all reactions of the type $(\tilde{p}, \tilde{n}(x-1)n)$ or $(\tilde{p}, \tilde{n}(x-1)nyp)$ are accounted for in the tellurium results, while reactions involving cascades of the type $(\tilde{p}, 2\tilde{n})$ or $(\tilde{p}, \tilde{n}\tilde{p})$, followed by evaporation, may become important for the yttrium case and could not be taken into account.

The right-hand side of Eq. (2) should be multiplied by N_{eff}, the effective number of target neutrons available for p-n charge-exchange interactions. Since N_{eff} is in general less than the total number of target neutrons, and is very difficult to estimate, this term was left out of Eq. (2). Values of $g(E^*)$ in the histograms illustrated in Fig. 8 are thus low by an unknown factor N_{eff}. However, this then permits the direct comparison of the area of the $g(E^*)$ distribution with the appropriate elementary p-n scattering cross section, since the effective number of target neutrons would increase both $g(E^*)$ and the total $(\tilde{p}, \tilde{n})$ cross sections.

The areas of the histograms in Fig. 8 are 13.0 and 14.1 mb, respectively. This compares with a value of 20.1 mb for the elementary p-n scattering cross section for c.m. scattering angles between $\frac{1}{2}\pi$ and π. Thus, approximately 65% for Y^{89} and 70% for Te^{126} of the total charge-exchange scattering is accounted for by $g(E^*)$. The remaining 30–35% of the charge-exchange scattering processes probably lead to longer cascades, which result in the deposition of larger excitation energies. There is no simple way of correcting the measured (p, xn) cross sections for these cases and thus the charge-exchange scattering probabilities illustrated represent only $(\tilde{p}, \tilde{n})$ cascades followed by nucleon evaporation.

ACKNOWLEDGMENTS

The authors wish to thank Dr. G. Friedlander for providing some of the results of the Vegas Monte Carlo calculations. They also wish to express their appreciation to Dr. F. M. Kiely for performing many of the evaporation calculations and writing the evaporation program, to A. C. Stalker for providing preliminary results of the p-n scattering kinematics, and to G. Smay for miscellaneous assistance. We also acknowledge the cooperation and assistance of the staff of the Carnegie-Mellon University Nuclear Research Center.